AIP Journal of Applied Physics

Observation of dislocations in diffused 4H–SiC p - i - n diodes by electron-beam induced current

S. Maximenko, S. Soloviev, D. Cherednichenko, and T. Sudarshan

Citation: Journal of Applied Physics **97**, 013533 (2005); doi: 10.1063/1.1828605
View online: http://dx.doi.org/10.1063/1.1828605
View Table of Contents: http://scitation.aip.org/content/aip/journal/jap/97/1?ver=pdfcov
Published by the AIP Publishing

Observation of dislocations in diffused 4H–SiC *p-i-n* diodes by electron-beam induced current

S. Maximenko,[a] S. Soloviev, D. Cherednichenko, and T. Sudarshan
Department of Electrical Engineering, University of South Carolina, Columbia, South Carolina 29208

(Received 23 July 2004; accepted 11 October 2004; published online 15 December 2004)

The electron-beam induced current (EBIC) method was employed to investigate the electrical activity of dislocations in silicon-carbide-diffused *p-n* diodes. It was observed that EBIC contrast depends on the type of defect (superscrew, screw, and edge dislocation). This dependence was attributed to spatial inhomogeneities in the electrical properties of the material around the dislocations due to different impurity-dislocation interactions during high-temperature (~1900 °C) diffusion. Chemical etching of the sample was used to define the nature of the defects observed by EBIC imaging. It was found that electrical breakdown of the diodes occurs at the location of superscrew dislocations. © *2005 American Institute of Physics*.
[DOI: 10.1063/1.1828605]

I. INTRODUCTION

Silicon carbide (SiC) is currently under intensive investigation as a promising material for high-power, high-frequency electronics and in radiation-hardened environments. Furthermore, electronic devices made from SiC can be used at much higher temperatures than those made from conventional semiconductors.[1] The suitability of SiC for these applications is due to its attractive physical properties such as high breakdown field, high saturated drift velocity, good radiation resistance, and high thermal conductivity. However, the presence of various crystallographic defects in commercially available material limits the wide commercialization of SiC devices.

This high density of defects (specifically threading dislocations, both screw and edge) has been a longstanding problem with SiC material. Screw dislocations in SiC can either be hollow or have a closed core depending on the magnitude of the Burgers vector.[2] The Burgers vector for hollow core screw dislocations (also known as superscrew dislocations) is two or more times the *c*-lattice constant for 6H–SiC, or three or more times the *c*-lattice constant for 4H–SiC.[3] Micropipes are known to significantly affect device characteristics such as leakage current and breakdown voltage in *p-n* and Schottky diodes.[4–6] Due to improvements in crystal-growth technology during the past several years, micropipe density has been significantly reduced to as low as 1.1 cm^{-2} for the highest quality 4H–SiC 2-in. wafers,[7] and it is likely that micropipes are totally eliminated within a few years. However, the dislocation density in good quality substrates is still high (10^3–10^4 cm^2). Low-voltage *p-n* and high-voltage Schottky diodes containing closed core screw dislocations exhibit a high reverse leakage current and low reverse breakdown voltage.[8,5] Threading edge dislocations can also compromise the performance of SiC devices although few studies have yet been reported. Moreover, no studies have been reported related to the effect of dislocations on the characteristics of the *p-n* diodes formed by diffusion, which is an alternate approach for the formation of *p* regions in SiC power devices.[9]

In this work, the electron-beam induced current (EBIC) technique was used for the identification and analysis of the electrical activity of screw, superscrew, and edge dislocations and their impact on the reverse characteristics of *p-n* SiC diodes.

II. EXPERIMENT

In this work, 4H–SiC 4° off-axis substrates oriented 4° toward the ⟨11-20⟩ direction with epi-films 12 μm thick with *n* doping of approximately 5×10^{15} cm^{-3} were purchased from CREE. The *p-i-n* diodes were formed by selective diffusion of aluminum and boron.[9] Diffusion was performed at a temperature of 1800–2000 °C in an argon ambient using a graphite mask with open windows from 200 to 1000 μm in diameter.[10] Standard photolithography process was employed to fabricate the planar *p-n* diodes structures without edge termination. Ohmic contacts with a thickness of 150 nm to the *p* region were fabricated by e-beam deposition of Ti/Al metal composition followed by rapid thermal process (RTP) annealing at 1000 °C for 5 min in nitrogen. Ohmic contact to the backside of the n^+ substrate was formed by deposition and annealing of Ni film.

Current–voltage characteristics of the fabricated diodes were measured using a Keithley 2410 voltage source measure unit. EBIC images of the formed diodes were obtained using a JOEL-35CF scanning electron microscope at an acceleration voltage of 25 kV and applied reverse bias varying in the range of 0–30 V. The EBIC observed defects were identified by chemical etching of the substrates in molten KOH at 600 °C. Mesa structures were formed by reactive ion etching to assist in locating the regions where the *p-i-n* diodes were formed after etching in order to compare those regions with the EBIC results and subsequent chemical etching.

[a]Electronic mail: maximens@engr.sc.edu

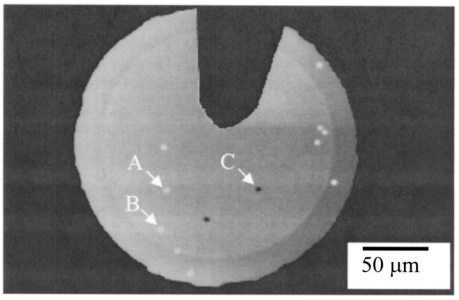

(a)

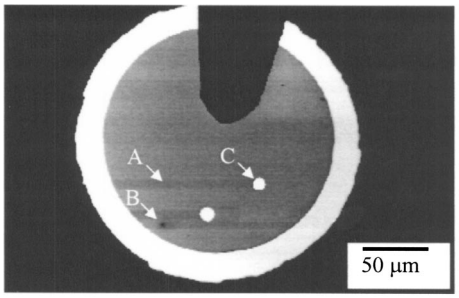

(b)

FIG. 1. EBIC image of a *p-i-n* diode under (a) 0 and (b) 20 V reverse bias.

III. RESULTS AND DISCUSSION

The EBIC image of a *p-i-n* diode under zero reverse bias is presented in Fig. 1(a). The inner circle represents the Ti/Al metal contact deposited on the *p* region. The uncovered *p* region (the outercircle) exhibits a darker EBIC image contrast at zero reverse bias.

At zero reverse bias, the EBIC image reveals defects as dark and bright contrast spots in the *p-n* diode area [Fig. 1(a)]. The degree of contrast generated by the defects in the EBIC image depends on the mechanism of recombination processes of the generated excess free charge carriers. The brighter regions correspond to area where the EBIC current is higher, while darker regions correspond to lower currents. Based on the modeling of EBIC contrast, variations in contrast are defined by the relationship between carrier lifetime at the defect, τ_d, and carrier lifetime in the surrounding region, τ. A dark contrast corresponds to a higher recombination rate at the defect ($\tau_d < \tau$), and a bright contrast corresponds to a lower recombination rate at the defect ($\tau_d > \tau$).[11] It has been shown in an earlier work that at high magnification, the bright spots observed in the EBIC images have bright halos with inner dark spots.[12] This type of contrast was attributed to the depleted zones of impurities around dislocations due to the gettering effect.[13]

Figure 1(b) shows the EBIC image of the same *p-i-n* diode as in Fig. 1(a) at a reverse bias of −20 V. The current contrast of the observed defects has significantly changed. Based on these images (at zero and −20 V biases), it was possible to distinguish three types of electrically active defects marked *A*, *B*, and *C* (see Fig. 1).

At zero bias, type *A* defects show a bright contrast, while at −20 V this type of defect disappears from the EBIC image. Type *B* defects (only one in this image) change contrast from bright at zero bias to dark at −20 V. Type *C* defects change contrast from dark at zero bias to bright at −20 V.

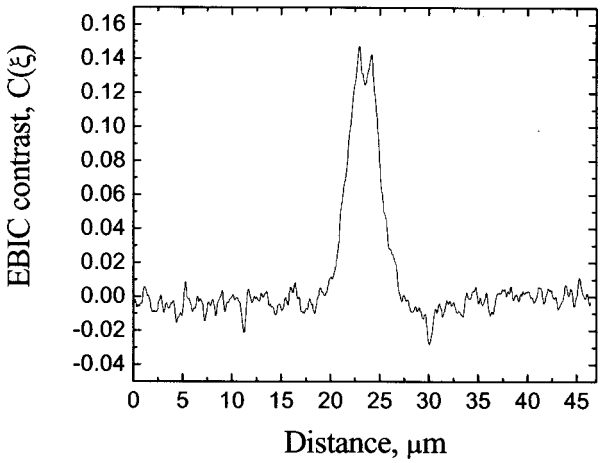

FIG. 2. Typical EBIC line scan for the type-*A* and type-*B* defects.

In order to analyze the contrast change, the EBIC current line scans across each defect were obtained as a function of applied reverse bias voltage. A defect contrast profile was calculated according to the expression

$$C(\xi) = \frac{I_d(\xi) - I_0}{I_0}, \text{ where } I_0 = I_d(\xi \to \infty),$$

where $I_d(\xi)$ is the peak EBIC current at the position of the defect, ξ is the distance between the e-beam scan line from the center of the defect (maximum signal or contrast is obtained for $\xi = 0$), and I_0 is the EBIC background signal. The contrast value $C(\xi)$ is negative for dark and positive for bright image contrasts. As mentioned earlier the defects type *A* and type *B* have bright halos with inner dark spots which can be resolved only by obtaining high-resolution EBIC images of the defects, where EBIC contrast from the dark inner spot is noticeably smaller than the bright halo as presented in Fig. 2 for zero bias.[12] At low-resolution scanning conducted in the present experiments, the contrast from the dark inner spot is smeared and the measured contrast profile is mostly defined by a bright halo signal corresponding to the central part of the defects. Figure 3 shows the maximum contrasts of specific defects (left scale) versus reverse bias voltage. Also, Fig. 3 presents the reverse *I–V* curve (right scale) of the *p-i-n* diode shown in Fig. 1.

It can be seen that the appearance of a dark contrast on defect *B* and an increase in the bright contrast on defect *C* correlate with an increased leakage current, as shown in Fig. 3. Note that the bright contrast of defect *C* gradually increases during the increase in reverse bias from around 7.5 to 22 V. A further increase in reverse bias decreases EBIC contrast and the signal from the defect becomes indistinguishable from the background noise.

In order to determine the type of defect observed by EBIC, the sample was etched in molten KOH. As is well known[14–18] chemical etching is a valuable tool for defect identification in SiC. By the shape of the etch pit it is possible to identify the nature of the defect.[19] The scanning electron microscopy (SEM) image of the device surface after

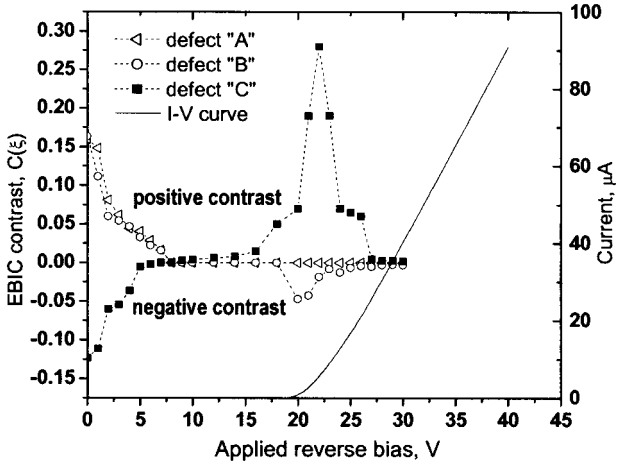

FIG. 3. Magnitude of maximum EBIC contrast as a function of applied reverse bias taken from a line scan across defects *A*, *B*, and *C* and reverse bias $I-V$ plot from the same diode.

etching is shown in Fig. 4. Comparison of the EBIC image taken at zero bias and the etch pit map demonstrates 100% correlation between revealed defects.

The etch pit configuration allows identification of three types of dislocations, correlated with three types of defects observed by EBIC contrast. High-resolution SEM images of these etch pits are presented in Fig. 5. Hexagonal etch pits with a dark center spot correlate with type *A* defects and are considered screw dislocations. Large hexagonal etch pits with a center hole correlate with type *B* defects or superscrew dislocations. Hexagonal etch pits correspond to type *C* defects and are edge dislocations which have been converted from basal plane dislocations in the substrate.[20] These results were confirmed by polishing the sample (removing the epilayer) after chemical etching and performing additional chemical etching. These procedures revealed basal plane dislocations in the region where the edge dislocation was prior to epitaxial layer removal (Fig. 6). Table I summarizes the observed EBIC contrast behavior of identified defects at different applied bias conditions.

To explain the EBIC contrast behavior, it was assumed that all defects are extended threading dislocations that have penetrated from the substrate into the epitaxial layer. The *p-n* junction depth formed by diffusion was around 4 μm. The penetration range of primary electrons, *R*, into the SiC was $\sim$4.5 μm calculated according to the expression

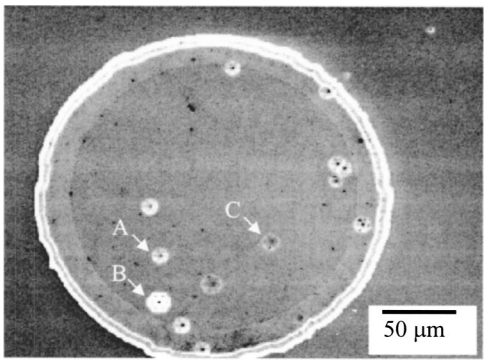

FIG. 4. SEM image of the etched *p-i-n* diode structure.

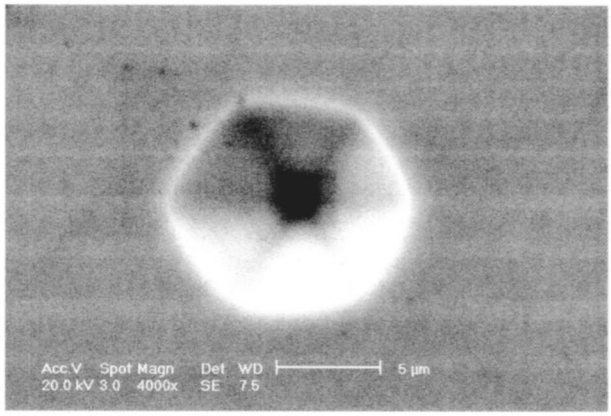

(a)

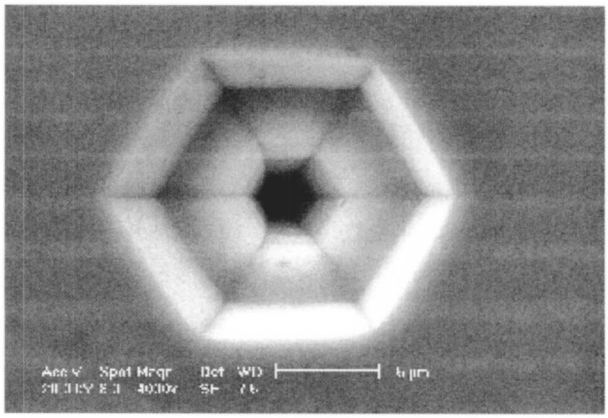

(b)

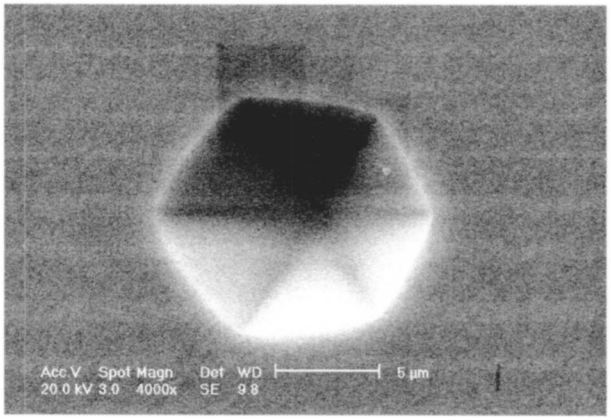

(c)

FIG. 5. High-resolution SEM image of three different types of etch pits found in tested sample: (a) type *A* screw, (b) type *B* superscrew, and (c) type *C* edge dislocations.

$R=(0.0276A/\rho\times Z^{0.889})E^{1.67}$ (where E is in keV, A is the atomic weight in g/mol, ρ is the SiC density in gm/cm^3, and Z is the atomic number)[21] for an accelerating voltage of 25 kV (taking into account electron scattering in metal film). Since the penetration range of primary electrons, *R*, is close to the depth of the *p-n* junction, the signal level from the substrate region is not significant. At low reverse bias condi-

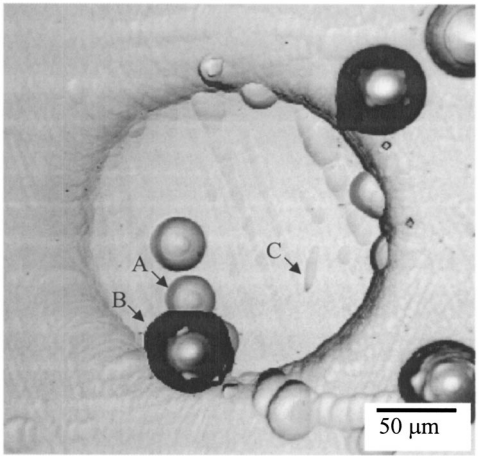

FIG. 6. Polishing and second chemical etching reveal basal plane dislocation.

tions, the dominant EBIC current is due to minority carriers generated in the *p*-diffused region with very little contribution from n^- drift region. With an increase in reverse bias voltage, the depletion width in the n^- drift region increases as well as the internal electric field in the depletion region that leads to an increase of the EBIC current.

Based on the results obtained, the electrical activity of dislocations in the diffused SiC *p-n* junction depends on the type of dislocation (superscrew, screw, or edge). Note that previous EBIC investigations of defects in SiC Schottky diodes did not demonstrate a visible impact of defect type on electrical activity.[22] Therefore, it appears that the impurity-dislocation interaction that occurs during high-temperature diffusion has a significant effect on the electrical behavior of the defects. Indeed it was shown that the electrical properties of dislocations in a semiconductor material such as Si are greatly influenced by their interactions with point defects.[23]

The impurity-dislocation interaction process is determined by the strain field around a dislocation and the nature of the defect. As a result it causes a spatially nonuniform impurity distribution around a defect site and this leads to local inhomogeneities in the electrical properties of the material around different types of dislocations as well as in the dislocation core region. Therefore the crystallographic structure of the defect itself has a significant influence on the EBIC contrast.[24]

The increase in the EBIC current for screw dislocations (defect *A* in Fig. 1) is attributed to depleted zones of impurities around the dislocations, which are formed due to "the gettering effect" during high-temperature diffusion (1800–2100 °C). This results in a brighter EBIC image contrast in the depleted zone because the carrier lifetime in the depleted zone is higher than the background carrier lifetime and, hence, a lower carrier recombination rate. At zero bias, the background recombination current is relatively low, thus, the EBIC signal is sensitive even to slight local fluctuations in doping concentration, which take place around screw dislocations. Under reverse bias, the generated carriers are mostly collected in the enlarged space-charge region of the *p-n* junction due to a higher electric field. Thus, the effect of the nonuniform doping distribution around screw dislocations on the resulting EBIC current becomes negligible and, hence, the bright contrast around screw dislocations disappears at reverse bias [Fig. 1(b)].

TABLE I. Observed EBIC contrast for the identified defects.

	Distinguishing features EBIC		
Defect type	Zero applied bias	With applied reverse bias	Defect
A	Bright contrast	No contrast	Screw dislocation
B	Bright contrast	Dark contrast	Superscrew dislocation
C	Dark contrast	Bright contrast	Converted edge dislocation

A superscrew dislocation is a hollow core screw dislocation with a Burgers vector two or more times the *c*-lattice constant for SiC.[25] Therefore an impurity-depleted zone would be expected to form around the hollow core screw dislocation as it would occur around closed core screw dislocations. Thus, a bright contrast at zero bias around superscrew dislocations can also be attributed to the gettering effect [defect *B* in Fig. 1(a)]. Under reverse bias, we believe that the recombination of excess charge carriers becomes dominant in the open core, which can be considered as an internal surface in the bulk material having a large number of dangling bonds.[26] This results in a change of EBIC contrast from bright to dark.

The homogenous dark EBIC contrast [defect *C* in Fig. 1(a)] from edge dislocations indicates that a depleted zone of the impurities was not formed around the edge dislocation during the diffusion process. An explanation for this is that the distance at which the impurity atoms are captured by a screw dislocation exceeds this distance for edge dislocations; $\eta = R_s/R_e \cong 3.3$ (where R_s is the "effective capture radius" for the screw dislocation and R_e for the edge dislocation).[27] Therefore, the depleted zone of the impurities that forms around an edge dislocation is significantly smaller than around screw dislocations. At reverse bias condition, the strong bright contrast can be explained in terms of the reemission of electrons captured by dangling bonds on the core of an edge dislocation induced by the high internal electric-field *p-n* space-charge region.

Moreover, it is worth noting that EBIC contrast depends on the atomic structure of the dislocation core in terms of the so-called Hooke's radius, which defines the distance from the dislocation core with essentially destroyed atomic lattice. The formation conditions of a thermodynamically stable dislocation with a hollow or closed core are different for screw and edge dislocations,[28] resulting in different Hooke's radii. The approximate value of the Hooke's radius for a closed core dislocation can be estimated as $r_h \cong b(\mu/4\times\pi^2\times U_0)^{1/2} \cong 0.5b$ (where μ is shear modulus, U_0 is the strain energy density at the center of the dislocation core, and b is the Burgers vector).[29] Thus, the interaction mechanism of free carriers with screw or edge dislocations is also expected to be different that can as well define their recombination activity dissimilarity.

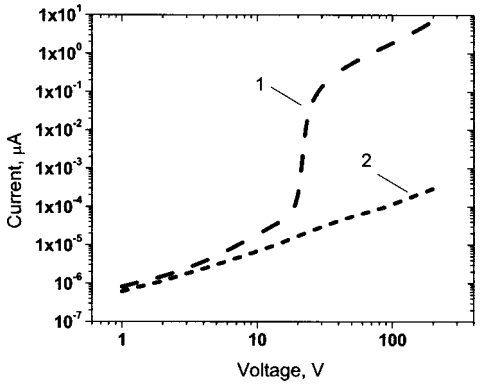

FIG. 7. Typical reverse current $I-V$ characteristics of p-i-n diodes containing (1) at least one superscrew dislocation and (2) without this defect.

In order to study the effect of these defects on device performance, reverse current–voltage measurements were performed. It was found that devices containing superscrew dislocations had a high leakage current and low breakdown voltage compared to devices without this kind of defect. Figure 7 shows typical reverse $I-V$ characteristics of devices with and without superscrew dislocations. Note that the $I-V$ curve of a diode with superscrew dislocation(s) has a characteristic knee at about 20 V in a log-scale plot. This can be explained by the fact that during high-temperature diffusion impurity atoms penetrate through the open core of a dislocation into the SiC substrate forming a p layer around the dislocation core which could bypass the n^- drift region. Thus, the region where breakdown occurs in diodes is associated with a superscrew dislocation. This is illustrated in Fig. 8 where a comparison of EBIC images at 0 [Fig. 8(a)] and applied reverse bias [Fig. 8(b)] identified the location of a superscrew dislocation, which was the site of breakdown after further testing of the device, as shown in Fig. 8(c).

IV. CONCLUSION

It has been shown that the EBIC mode of SEM can be used to identify different types of defects in SiC-diffused p-n diodes. At zero bias, screw and edge dislocations exhibited different EBIC contrasts (bright and dark) while screw and superscrew dislocations exhibited similar contrasts. Applied reverse bias to the structure drastically changed the EBIC contrast of the defects. Superscrew dislocations changed from a bright contrast to dark, while the screw dislocation contrast darkened to the background signal. Edge dislocation contrast changed from dark to bright. These characteristic changes permitted identification of the type of dislocation present in the diffused p-i-n structure and were explained in terms of differences in defect structure and defect-impurity interactions. Local junction breakdown effects and a high leakage current of the tested structures associated with the superscrew dislocations were also observed.

ACKNOWLEDGMENTS

We are grateful to Dr. C. Wood for his interest and support of this research. This work was supported by ONR, Grant No. 000140310584. We thank A. Grekov and Dr. Y. Gao for their assistance in providing the p-i-n diode test structures for this study. We also thank Julie Morris for her assistance in the preparation of this manuscript.

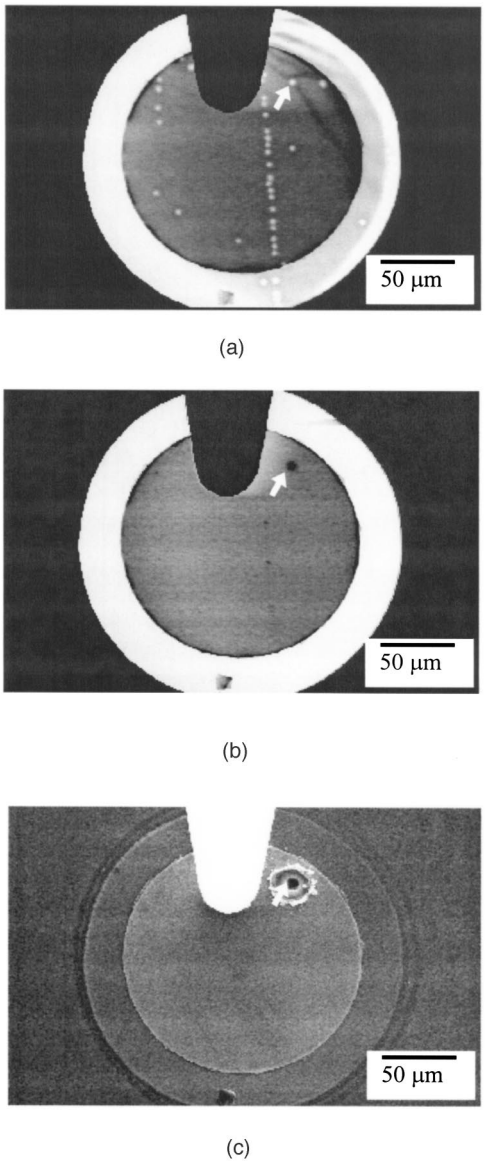

FIG. 8. EBIC image of a p-i-n diode at (a) 0 and (b) 20 V applied reverse bias. (c) SEM image of the p-i-n surface after breakdown at the superscrew dislocation. The arrow shows the defect site and place of breakdown.

[1] P. Masri, Surf. Sci. Rep. **48**, 1 (2002).
[2] J. Heindl, H. P. Strunk, V. D. Heydemann, and G. Pensl, Phys. Status Solidi A **162**, 251 (1997).
[3] W. M. Vetter and M. Dudley, J. Appl. Phys. **96**, 348 (2004).
[4] J. Powell, P. Neudeck, D. Larkin, J. Yang, and P. Pirouz, Inst. Phys. Conf. Ser. **137**, 161 (1993).
[5] Q. Wahab, A. Ellison, A. Henry, E. Janzén, C. Hallin, J. Di Persio, and R. Martinez, Appl. Phys. Lett. **76**, 2725 (2000).
[6] P. Neudeck and J. Powell, IEEE Electron Device Lett. **15**, 63 (1994).
[7] St. G. Muller *et al.*, J. Cryst. Growth **211**, 325 (2000).
[8] P. Neudeck, IEEE Trans. Electron Devices **46**, 478 (1999).
[9] Y. Gao, S. Soloviev, C. C. Tin, and T. S. Sudarshan, J. Appl. Phys. **90**, 5647 (2001).
[10] S. Soloviev, Y. Gao, X. Wang, and T. S. Sudarshan, J. Electron. Mater. **30**, 224 (2001).
[11] H. J. Leamy, J. Appl. Phys. **53**, R51 (1982).
[12] S. Maximenko, S. Soloviev, D. Cherednichenko, and T. Sudarshan, Appl. Phys. Lett. **84**, 1576 (2004).

[13]C. Frigeri, Mater. Sci. Eng., B **20**, 175 (1993).
[14]S. Amelinckx and G. Strumane, J. Appl. Phys. **31**, 1359 (1960).
[15]J. Takahashi, M. Kanaya, and Y. Fujiwara, J. Cryst. Growth **135**, 61 (1994).
[16]J. Takahashi, N. Ohtani, and M. Kanaya, J. Cryst. Growth **167**, 596 (1996).
[17]E. K. Sanchez, J. Q. Liu, M. De Graef, M. Skowronski, W. M. Vetter, and M. Dudley, J. Appl. Phys. **91**, 1143 (2002).
[18]R. Yakimova, A.-L. Hylén, M. Tuominen, M. Syväjärvi, and E. Janzén, Diamond Relat. Mater. **6**, 1456 (1997).
[19]S. Ha, Mater. Sci. Forum **389–393**, 443 (2002).
[20]T. Ohno, H. Yamaguchi, S. Kuroda, K. Kojima, T. Suzuki, and K. Arai, J. Cryst. Growth **260**, 209 (2004).
[21]K. Kanaya and S. Okayama, J. Phys. D **5**, 43 (1972).
[22]C. M. Schnabel, M. Tabib-Azar, P. G. Neudeck, S. G. Bailey, H. B. Su, M. Dudley, and R. P. Raffaele, Mater. Sci. Forum **338–342**, 489 (2000).
[23]E. B. Yakimov, J. Phys. III **7**, 2293 (1997).
[24]K. Simino, Phys. Status Solidi A **171**, 111 (1999).
[25]X. R. Huang, M. Dudley, W. M. Vetter, W. Huang, W. Si, and C. H. Carter, Jr., J. Appl. Crystallogr. **32**, 516 (1999).
[26]M. Haugk *et al.*, Phys. Status Solidi B **217**, 473 (2000).
[27]F. S. Ham, J. Appl. Phys. **30**, 915 (1959).
[28]B. Van Der Hoek, J. P. Van Der Eerden, and P. Bennerna, J. Cryst. Growth **56**, 621 (1982).
[29]D. I. Cherednichenko, Y. I. Khlebnikov, I. I. Khlebnikov, R. V. Drachev, and T. S. Sudarshan, J. Appl. Phys. **89**, 4139 (2001).